

Research Article

Open Access



Amorphous diamond embedded in dense boron nitride with excellent mechanical properties

Junkai Li¹, Guoliang Niu¹, Peiyang Mu¹, Bingmin Yan¹, Fuyang Liu¹, Shijing Zhao¹, Leiming Fang², Huiyang Gou¹

¹Center for High Pressure Science and Technology Advanced Research, Beijing 100193, China.

²Key Laboratory for Neutron Physics, Institute of Nuclear Physics and Chemistry, China Academy of Engineering Physics, Mianyang 621900, Sichuan, China.

Correspondence to: Dr. Huiyang Gou, Center for High Pressure Science and Technology Advanced Research, 10 Xibeiwang East Rd., Haidian District, Beijing 100193, China. E-mail: huiyang.gou@hpstar.ac.cn; Dr. Junkai Li, Center for High Pressure Science and Technology Advanced Research, 10 Xibeiwang East Rd., Haidian District, Beijing 100193, China. E-mail: junkai.li@hpstar.ac.cn

How to cite this article: Li J, Niu G, Mu P, Yan B, Liu F, Zhao S, Fang L, Gou H. Amorphous diamond embedded in dense boron nitride with excellent mechanical properties. *Microstructures* 2024;4:2024010. <https://dx.doi.org/10.20517/microstructures.2023.54>

Received: 28 Sep 2023 **First Decision:** 31 Oct 2023 **Revised:** 19 Dec 2023 **Accepted:** 25 Dec 2023 **Published:** 8 Feb 2024

Academic Editor: Daolun Chen **Copy Editor:** Fangling Lan **Production Editor:** Fangling Lan

Abstract

Diamond and cubic boron nitride (BN) are important materials with a variety of technological and industrial applications; however, overcoming the intrinsic brittleness of these materials is still a challenge. Here, we synthesize a compound of crystalline BN and amorphous diamond-like carbon through BN nanotubes and fullerene under high pressure and high temperature conditions. The obtained composite exhibits excellent combination of a measured Vickers' hardness of 86.2 GPa and fracture toughness of 10.2 MPa m^{1/2}. Morphological and structural characterizations reveal that the amorphous diamond-like carbon is homogeneously embedded in a matrix of dense BN. The formation of the amorphous diamond-like carbon particles within the polycrystalline BN can effectively impede the migration of crack tips when the compound is cracking, in which most of crack tips are forced to deflect or confined near the boundaries of dense BN and amorphous diamond particles. The crystalline-amorphous composite strengthening presented here may provide a promising strategy for the further improvement of mechanical properties of hard or superhard materials.

Keywords: Superhard materials, HPHT synthesis, boron nitride, amorphous diamond-like carbon

INTRODUCTION

Superhard materials, for example cubic boron nitride (c-BN) and diamond, are an interesting class of



© The Author(s) 2024. **Open Access** This article is licensed under a Creative Commons Attribution 4.0 International License (<https://creativecommons.org/licenses/by/4.0/>), which permits unrestricted use, sharing, adaptation, distribution and reproduction in any medium or format, for any purpose, even commercially, as long as you give appropriate credit to the original author(s) and the source, provide a link to the Creative Commons license, and indicate if changes were made.



materials that play a decisive role in the field of materials processing. The application of superhard materials as the cutting tools has promoted the prosperity of high-precision materials processing such as aerospace and mechanical manufacturing^[1-5]. Among superhard materials, c-BN exhibits excellent thermal stability and chemical inertness, demonstrating extraordinary practicality in high-speed cutting, especially for the cutting of ferrous metals^[6-8]. However, the Vickers' hardness of single crystal c-BN is approximately half that of natural diamond. For decades, great efforts have been devoted to improving the mechanical properties, including Vickers' hardness and fracture toughness; the grain boundary strengthening and twin strengthening are demonstrated to be the effective strategies for the improvement of mechanical properties of the materials^[9,10]. Grain boundary strengthening is achieved by reducing grain size to increase the density of grain boundaries, thereby limiting dislocation movement. When the grain sizes decrease to the nanoscale, the hardness of the material will be increased significantly. The nanopolycrystalline state of c-BN shows a Vickers' hardness almost twice that of a single crystal^[11-14]. However, the calculations reveal that grain boundary strengthening is effective up to a threshold of eight nanometers. Below this size, an inverse Hall-Petch effect occurs, leading to the failure of the grain boundary strengthening^[15,16]. Nevertheless, twinning strengthening can operate even at sub-nanoscale levels. Notably, the hardness of c-BN with an average twin domain size of 3.4 nm surpasses that of natural diamond^[17]. In industrial applications, it remains a challenge to prepare bulk materials with a high proportion and uniformly distributed twin structure. As a result, grain boundary strengthening continues to be the most widely used method in the industry. Enhancing the Vickers' hardness and fracture toughness of polycrystalline boron nitride has always been a research focus. Due to its inherent cleavage feature, c-BN exhibits the brittleness and is prone to premature failure. Therefore, a new strengthening method is highly needed to improve the mechanical properties of c-BN^[18,19].

Amorphous materials have a fundamentally different structure from crystalline materials and do not possess defects such as grain boundaries, dislocations, and twins^[20-22]. As a result, the fracture behavior of amorphous materials differs from that of crystalline materials. Since the amorphous form is a state of disordered arrangement of atoms, free volume exists between atoms, and plastic deformation of amorphous alloys generally occurs in the form of shear bands^[23-25]. According to literature, the hardness of amorphous diamond-like carbon materials can scratch natural diamonds, demonstrating excellent mechanical properties^[26].

Based on the difference in strengthening mechanisms between polycrystalline and amorphous materials, it is particularly important to construct a crystal/amorphous superhard material system and study the relationship between its mechanical properties and structure. The amorphous/crystalline strategy may provide a promising way to achieve the high strength of materials that can resist deformation and improve mechanical performance. Despite the extensive successes of preparations of crystalline diamond/c-BN composites, there is no exploration about amorphous-crystalline compounds of amorphous diamond-like carbon and boron nitride^[27-30].

In this study, we utilized hexagonal boron nitride nanotubes (BNNTs) and C₆₀ as precursors to investigate the structural and microstructural evolutions after high pressure and high temperature (HPHT) treatment. Hexagonal boron nitride (h-BN) undergoes a gradual transformation into a composite material consisting of wurtzite boron nitride (w-BN) and c-BN and subsequently transitions into pure c-BN. Moreover, fullerene (C₆₀) is converted into amorphous carbon and then ultimately crystallizes into diamond. The compound of crystalline c-BN and amorphous diamond-like carbon is obtained to have the excellent combination of Vickers' hardness and fracture toughness. The analysis shows that when cracking, the migration of the crack tip will be blocked by the amorphous diamond-like carbon particles, and the dislocation activities are hindered by the interface of crystalline c-BN and amorphous diamond-like carbon.

The present results may offer an effective strategy of crystalline/amorphous compounds for further strengthening of superhard materials.

MATERIALS AND METHODS

Multi-walled BNNTs with 99.9% purity were purchased from Nanjing Xianfeng Nanomaterials Co., Ltd. Fullerene was obtained from Macklin Reagent Co., Ltd. [Supplementary Figure 1A](#) and [B](#) depicts the X-ray diffraction (XRD) patterns of C₆₀ fullerene and BNNTs, respectively. The diffraction peaks of C₆₀ fullerene align with the standard card (JCPDS No. 79-1715), signifying high crystallinity. In addition, the diffraction peaks of the BNNTs align with the standard card (JCPDS No. 73-2095) for h-BN. The nanotubes exhibit the inner and outer diameters of 20 and 50 nm, respectively, and the lengths vary from a few micrometers to tens of micrometers [[Supplementary Figure 1C](#) and [D](#)]. Moreover, the selected area electron diffraction (SAED) and high-resolution TEM (HR-TEM) image confirm the high quality of C₆₀ [[Supplementary Figure 1E](#) and [F](#)]. The precursor was prepared by grinding BNNTs and C₆₀ in a 4:1 mass ratio for 30 min in a mortar. The resulting mixture was then pre-pressed into a cylindrical shape with a diameter of 1.6 mm and a length of 2 mm. The experiments were conducted using a Kawai-type multi-anvil press (1,500-ton). Tungsten carbide anvils with a truncation of 3 mm and a side length of 10 inches (25.4 cm) were used in the experiments. The schematic diagram of the high-pressure and high-temperature experimental process is presented in [Supplementary Figure 2](#). The pressure was slowly increased by 1 bar/min to the target pressure. The heating was performed in a constant power mode with a heating rate of approximately 100 °C/min. Real-time temperature monitoring during the experiment was achieved using a D-type thermocouple made (W3%Re-W25%Re), which enabled temperature measurements up to 2,300 °C under high pressure. Once the target temperature was reached, the sample was allowed to continue heating for 10 minutes before the heating was stopped by turning off the power. The pressure was then slowly released at a rate of 0.5 bar/min. The resulting sample was embedded in resin or rosin and polished using diamond papers with progressively finer particle sizes of 15, 9, 5, 3, and 1 μm. The polished sample was then cleaned using ultrasonic waves with anhydrous ethanol and air-dried in preparation for subsequent characterization.

Mechanical properties were tested using a micro-hardness tester (Qness Q60A+) with a load range of 0.1-5 kg. The instrument was pre-calibrated using a standard block, and then different loads were applied to the sample for single-point testing, with five valid data points collected for each load. Finally, the data for different loads were summarized.

The mechanical properties of the samples were also measured using a Nano Indenter G200 XP, employing Berkovich indenters and the continuous stiffness measurement (CSM) method. The maximum depth of indentation was set to 800 nm. In order to ensure representative results, we carefully selected five different regions and obtained three data points within each region. At least five valid points were collected for subsequent analysis and processing^[31].

The hardness of the material was calculated using Equation 1, where F (in Newtons) represents the applied load, and L (in micrometers) denotes the arithmetic mean of the two diagonals of the Vickers indentation^[32].

$$Hv = \frac{1854.4F}{L^2} \quad (1)$$

The fracture toughness of the material is calculated using Equation 2, where F (in Newtons) represents the applied load, and C corresponds to the arithmetic square root of the distance from the center of the indentation to the tip of the crack^[33].

$$K_{IC} = \frac{0.0742F}{c^{1.5}} \quad (2)$$

Structure characterization was performed using an X-ray diffractometer (D8 Discover, Bruker) equipped with a Cu K α radiation X-ray source ($\lambda = 1.54056 \text{ \AA}$). Morphological analysis was conducted using scanning electron microscopy (FESEM, JSM-7900F) at an accelerating voltage of 15 kV and a working distance of 10 mm. A Pt coating was applied to the sample to minimize charge accumulation on the surface for better electrical conductivity.

A transmission electronic microscope (TEM, JMS-F200) was used for the characterization, with an accelerating voltage of 200 kV. The powder sample was dispersed in ethanol and subjected to ultrasonic processing to create a homogeneous suspension. The suspension was then dropped onto a copper grid and allowed to undergo complete ethanol evaporation. HR-TEM and SAED were utilized to characterize the morphology and structure of the sample. Electron energy loss spectroscopy (EELS) was performed using a spherical aberration-corrected TEM with an accelerating voltage of 300 kV. The sample was prepared using a focused ion beam (FIB) technique on a Scios Dual Beam instrument from Thermo Fisher. Gallium ions were used for grinding and cutting, and thinning was carried out under a beam current of 20-40 pA at 30 kV. The amorphous layer on the sample surface was removed using 5 kV 30 pA and 3 kV 30 pA, resulting in a final sample thickness of approximately 80 nm.

RESULTS AND DISCUSSION

As depicted in [Figure 1A](#), the diffraction peaks of the sample recovered at 25 GPa and 500 °C support the presence of both w-BN and h-BN, suggesting the phase transformation of h-BN into w-BN^[34,35]. The observed broadening of diffraction peaks indicates the disordered feature of the recovered samples at 25 GPa and 500 °C. With the temperature increases, the characteristic peak of (002) for h-BN gradually shifts to a higher angle, indicating a reduction of lattice distances, for example, the (002) plane of h-BN from 0.33 nm to approximately 0.31 nm.

The transformation of boron nitride resembles the conversion of graphite into diamond and involves an intermediate structure known as “compressed graphite”^[36]. When the temperature reaches 1,400 °C, the characteristic peak of h-BN disappears, indicating the completion of the transformation of boron nitride into its dense phases (w-BN and c-BN) in the recovered samples. However, there are no characteristic diffraction peaks of C₆₀ found in the temperature range from 1,000 to 1,600 °C, confirming the amorphous structure of carbon throughout the process. A composite of polycrystalline diamond and c-BN is obtained for the samples at 25 GPa and 1,800 °C, as seen by the (111) and (220) diffraction peaks of c-BN and the adjacent (111) and (220) diffraction peaks of polycrystalline diamond^[37,38].

The Vickers hardness of the recovered samples at 25 GPa and the temperature from 1,000 to 1,800 °C are estimated using a hardness tester with a load of 9.8 N. As shown in [Figure 1B](#) and [C](#), the Vickers hardness of the samples increases gradually from 1,000 to 1,400 °C. As shown in [Supplementary Figure 3](#), the recovered samples at 1,400 °C achieve an asymptotic hardness of around 86.2 GPa at approximate 8 N load [[Supplementary Figure 4](#)], harder than polycrystalline w-BN and polycrystalline c-BN^[30,39]. The increase in hardness is attributed to the transformation of non-dense boron nitride (h-BN and compressed h-BN) into dense-phase boron nitride. Above 1,400 °C, the hardness gradually decreases from 86.2 to 65.3 GPa. The fracture toughness of the composite exhibits a similar trend from 1,000 to 1,400 °C; the toughness gradually increases from 7.06 MPa m^{1/2} to 10.2 MPa m^{1/2} and then decreases to 7.55 MPa m^{1/2}. The maximum toughness of the sample presented, about 10.2 MPa m^{1/2}, is more than twice that of micrometer-sized polycrystalline c-BN^[11]. Notably, at the temperatures above 1,400 °C, both amorphous diamond-like carbon

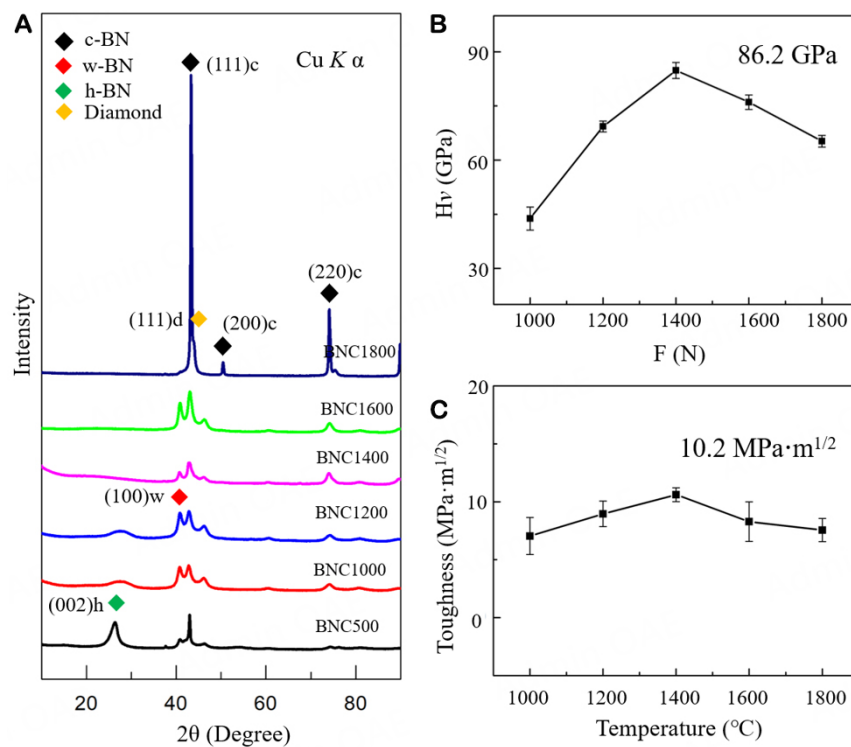


Figure 1. XRD patterns (A), the characteristic diffraction peaks of different phases (marked with different colors) and mechanical properties [Vickers' Hardness (B) and Fracture Toughness (C)] of recovered samples sintered at 25 GPa and 500-1,800 °C, named as BNCT (T represent temperatures).

and boron nitride gradually transform into the crystalline states, which may suggest the changes of the strengthening mechanism from the crystalline-amorphous system to the crystalline-crystalline system. Figure 2 presents the results of the nanoindentation tests conducted on the samples. The sample obtained at 1,200 °C exhibited a hardness and Young's modulus of approximately 85 and 810 GPa, respectively, at an applied load of approximately 100 mN. This can be attributed to the presence of non-dense phase boron nitride within the material. In addition, the sample obtained at 1,400 °C demonstrated a higher hardness and Young's modulus, measuring around 110 and 1,300 GPa, respectively, under the same test conditions. The enhanced values may be attributed to the complete transformation of the non-dense phases into its dense phase at high temperatures.

However, when the reaction temperature was increased to 1,800 °C, a notable reduction in both hardness and toughness was observed. The average values for hardness and Young's modulus were measured at approximately 92 and 900 GPa, respectively. XRD analysis indicated that the sample obtained at 1,400 °C represented an amorphous-crystalline system, while the sample obtained at 1,800 °C exhibited a composite polycrystalline system.

Supplementary Figure 3 depicts the typical load-displacement curves obtained from the nanoindentations conducted on the samples. The loading and unloading curves exhibit a smooth behavior, indicating highly reliable indentation results. In Supplementary Figure 3B, the maximum deformation depths after elastic unloading are presented for three samples, measuring at 152.6, 185.3 and 216.2 nm, respectively. This suggests that the sample obtained at 1,400 °C exhibits the highest resistance^[40,41].

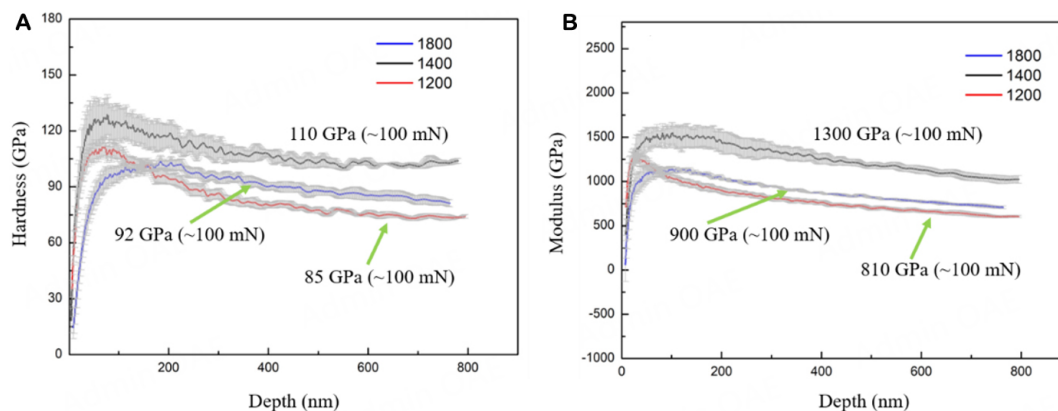


Figure 2. Nanoindentation test results of different samples. (A) Hardness and (B) Young modulus, with error bar (gray), respectively (the curve labels refer to the temperature at which samples were quenched; e.g., 1,400 represents the sample obtained at 1,400 °C).

Supplementary Figure 3C and D demonstrates a “pop-in” phenomenon observed during the loading process of the samples obtained at 1,400 and 1,800 °C. In the case of single crystals, this phenomenon is typically associated with the indentation and crystal orientation^[42]. However, since the synthesized samples are isotropic, it is likely that this “pop-in” effect is caused by the breakage of the second phase. Previous research indicates that the “pop-in” phenomenon is attributed to localized strength aging within the bulk material, which suggests a correlation with the diamond-like carbon present in the samples^[43]. Furthermore, a comparison reveals the distinct slopes in the pop-in curves between the 1,400 and 1,800 °C samples, potentially indicating differences in the materials’ ability to resist cracking.

The microstructure of the recovered samples was examined using SEM and TEM. For the sample obtained at 25 GPa and 1,000 °C [Figure 3A and B], boron nitride displays a turbostratic structure; C₆₀ presents an amorphous state, and the particle size of carbon is about 3.16 nm [Supplementary Figure 5]. SAED analysis indicates a mixture of “compressed h-BN” and dense boron nitride with amorphous carbon. The diffraction ring corresponding to the (002) base plane of “compressed h-BN” exhibits a significant broadening compared to the crystalline h-BN^[36]. The “compressed h-BN” is found to have a lamellar morphology. Additionally, a significant portion of the boundary area with amorphous carbon and the “compressed h-BN” is observed, which further decreases the hardness and toughness. For the sample obtained at 1,200 °C and 25 GPa [Figure 3C and D], we find that the majority of the area consists of a combination of the dense boron nitride and amorphous carbon, with only a small amount of “compressed h-BN”. The increase in the proportion of dense boron nitride strengthens the hardness of the samples. For the samples at 1,400 °C and 25 GPa [Figure 3E and F], SAED supports the presence of w-BN and c-BN. Additionally, carbon transforms into amorphous diamond-like carbon, as indicated by a distinct halo in the region of the diamond ring positions. However, the samples obtained at 1,800 °C transform into a polycrystalline compound [Figure 3G and H]. SAED reveals the presence of a complex of polycrystalline diamond and c-BN, which is further supported by XRD results. It is noted that the crystal-crystal system was found to exhibit lower mechanical properties than that of the crystal-amorphous system, which may be attributed to the different fracture mechanisms between them. In a crystal-amorphous system, the unique structure and combination of crystals and amorphous materials have a strengthening effect on the bulk material.

Elemental mapping was conducted on the sample obtained at 500 °C, revealing a uniform distribution of carbon within the boron nitride framework. The results are displayed in Supplementary Figure 6, where a curved tubular shape is visible, suggesting that the transformation of BNNTs into their dense phase is not

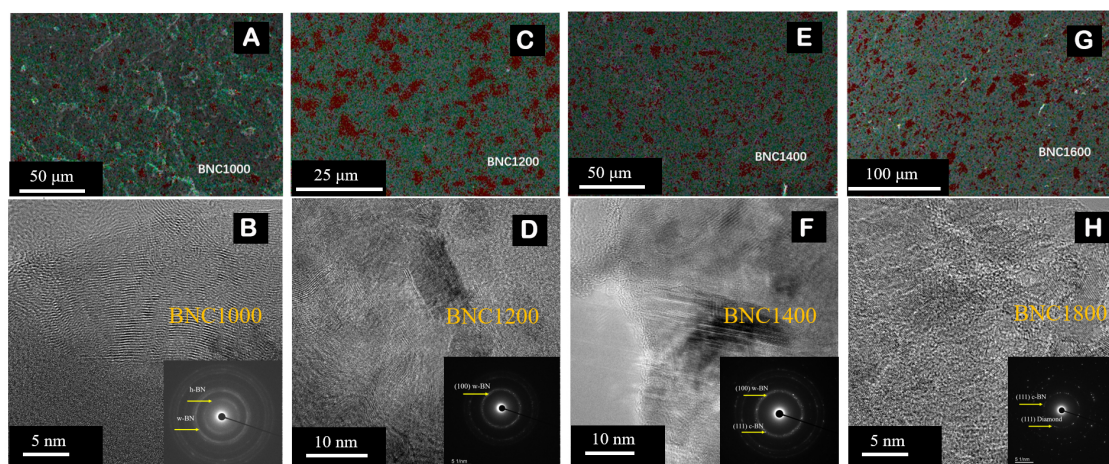


Figure 3. (A, C, E, G) SEM-EDS images of recovered samples at 25 GPa and different temperatures of 1,000-1,600 °C (red represents carbon element, green represents boron element, and blue represents nitrogen element); (B, D, F, H) TEM images and SAED patterns of recovered samples at different temperatures, 25 GPa 1,000-1,800 °C.

completed. This observation aligns with the XRD findings. Upon increasing the temperature to 1,200 °C, the morphology of the sample exhibits a crystalline-amorphous state, as depicted in [Figure 4A](#). The carbon particles with the crystal sizes of about 0.5-2 μm are embedded in dense boron nitride. The boundaries between the two phases can be seen in [Figure 4B](#), where the crystalline phase is of w-BN structure. The carbon region shows a disordered atomic structure. The Fourier transform image of the amorphous carbon region exhibits a characteristic ring halo, rather than discrete diffraction peaks [[Figure 4C](#)]. Meanwhile, the carbon region can be clearly distinguished by TEM-EDS mapping [[Figure 4D-F](#)].

[Figure 5A](#) displays a TEM image showing the boundary between the amorphous and crystalline phases. Different regions are selected for selected area electron diffraction (SAED). In [Figure 5B](#), the SAED pattern is corresponding to the black circular area in [Figure 5A](#), representing the two-phase region. In [Figure 5C](#), the SAED pattern of the crystalline region (red circular area) suggests the presence of both w-BN and c-BN phases in this area. [Figure 5D](#) shows the SAED pattern of the amorphous region (yellow circular area), where the amorphous halo appears blurred. Notably, there is a correlation between the halo region and the diffraction position of crystal diamond. Additionally, the amorphous halo in the carbon region corresponds to amorphous diamond-like carbon. Further analysis was conducted using a spherical aberration-corrected TEM equipped with EELS. [Figure 5E](#) and [F](#) illustrates the EELS results for the crystalline boron nitride and amorphous carbon regions, respectively. In [Figure 5E](#), the peak position of the EELS spectrum at about 197 eV represents the $1s-\sigma^*$ loss peak of the B element, indicating the sp^3 bonding between boron and nitrogen. In [Figure 5F](#), the clear peak position for the C element EELS spectrum is located at 293 eV, which is the $1s-\sigma^*$ loss peak of the C element. The $1s-\pi^*$ loss peak does not appear at the position of 285 eV, indicating a sp^3 bonding^[44,45]. The results demonstrate that the samples obtained at 25 GPa 1,400 °C are a compound of dense boron nitride and amorphous diamond-like carbon.

The materials usually crack when they are impacted by a large load, beyond a critical point of tolerance limit, the fracture occurs and the materials break. [Figure 6A-D](#) shows the indentations and cracks of the samples after indentation tests. Notably, the cracks observed for the sample at 1,200 °C [[Figure 6A](#)] are relatively longer and the bending occurred during crack propagation, which indicate that the more severe fractures are required to release the energy, likely due to the presence of a non-dense phase within the material. Nevertheless, the observed cracks become shorter in the samples of 1,400 °C [[Figure 6B](#)] and 1,600

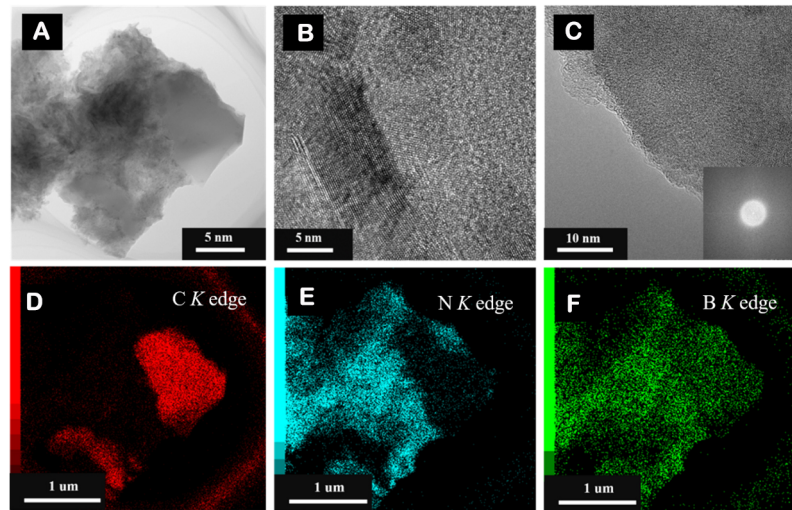


Figure 4. TEM images of the samples obtained at 1,200 °C; (A) Composite of amorphous carbon and boron nitride (B) Zooming in image of boundary (w-BN and amorphous diamond-like carbon); (C) Zooming in image of amorphous diamond-like carbon area and Fourier transform diagram; (D-F) EDS mapping of Figure 3A, green represent boron, blue represent nitrogen, and red represent carbon.

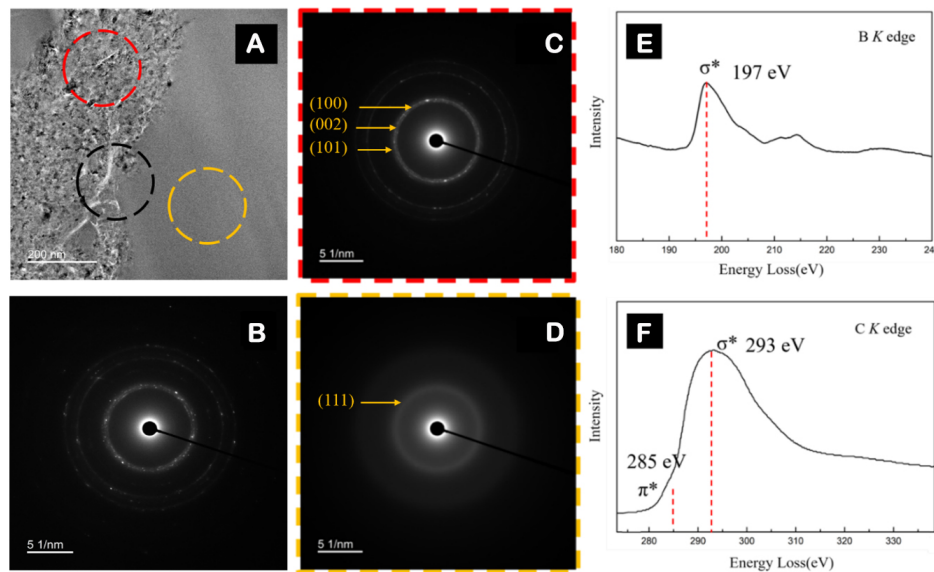


Figure 5. SAED and HRTEM images of samples obtained at 25 GPa 1,400 °C, (A) TEM image of crystalline-amorphous boundary; (B) Diffraction pattern of amorphous-crystalline phases (black cycle region); (C) Diffraction pattern of crystalline region (red cycle region); (D) Diffraction pattern of amorphous region (yellow cycle region); (E and F) EELS spectrum of boron and carbon.

°C [Figure 6C], suggesting that the energy can be rapidly released upon indentation and cause a smaller cracks. This phenomenon can be attributed to the formation of crystal/amorphous composite. For the recovered sample at 1,800 °C, however, a direct break observed under the same load [Figure 6D] indicates that the crystal-crystal system is not as effective as a crystal-amorphous system in improving mechanical properties.

To gain a deep understanding of the excellent mechanical properties of the samples with the crystalline-amorphous structure, further investigations are conducted using TEM to observe crack extension at the

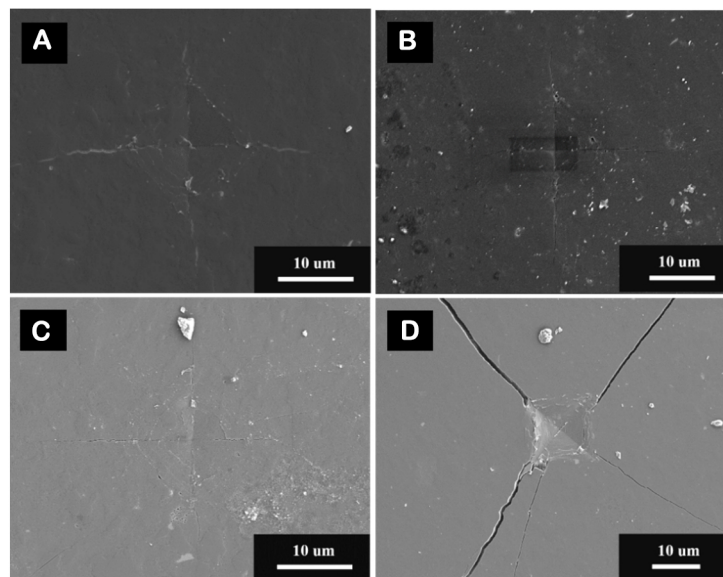


Figure 6. SEM images of the indentation area (load: 9.8N); recovered samples synthesized at 25 GPa, 1,200 °C (A), 1,400 °C (B), 1,600 °C (C), 1,800 °C (D).

nanoscale. Elemental mapping of the sample obtained at 1,200 °C is presented in [Supplementary Figure 7](#). Within the figure, a noticeable crack can be observed traversing through both the boron nitride and carbon regions, which indicates that the harder diamond-like carbon particles are insufficient to resist fracture. The EELS spectra of the K-edge absorption of boron and carbon in the 1,200 °C sample in [Supplementary Figure 8](#) reveal the presence of sp^2 bonds, suggesting the existence of non-dense phases in the system. This non-dense phase is a contributing factor to the lower mechanical strength of the bulk material.

In [Supplementary Figures 9 and 10](#), cracks in the samples at 1,400 °C are only observed in the boron nitride region, and most of cracks are blocked at the boundaries between carbon and boron nitride. This observation explains the high hardness of the sample, as the diamond-like carbon particles effectively inhibit crack tip migration. The EELS spectrum in [Supplementary Figure 8](#) indicates that at 1,400 °C, boron nitride has completely transformed into sp^3 bonding, and almost all of the carbon elements are also bonded by sp^3 bonds. For the sample obtained at 1,800 °C, the EELS spectrum reveals that all carbon and boron nitride in the sample are sp^3 bonded, as shown in [Supplementary Figure 8](#). The sample obtained at 1,800 °C represents a composite consisting of polycrystalline diamond and c-BN. [Supplementary Figure 11](#) demonstrates cracks in both the boron nitride and carbon regions. Polycrystalline diamond and boron nitride composites are reinforced by grain boundaries.

As shown in the [Supplementary Figure 11](#), there was no phenomenon of large angle deviation or obstruction of cracks when the crack tip migrated to the boundaries of crystal diamond and c-BN.

Polycrystalline diamond and c-BN composites are reinforced by grain boundaries. Remarkably, in the observed figure, no significant occurrence of large-angle deviation or crack obstruction was noted when the crack tip traversed the boundaries between the crystal diamond and c-BN. This finding suggests that the migration of crack tips toward these boundaries proceeded smoothly without encountering substantial obstacles or deviations.

This phenomenon explains the cracking of the bulk sample under higher load for the sample obtained at 25 GPa 1,800 °C, the material exhibits intrinsic brittleness, as shown in [Figure 6D](#). Comparing the different samples, it can be inferred that the polycrystalline composite exhibits lower fracture resistance compared to the polycrystalline amorphous composite.

It is well-known that crack tip migration in polycrystalline materials is impeded by grain boundaries^[46]. In the case of crystalline-amorphous compounds, when the crack tips reach the boundaries between the amorphous and crystalline regions, if the energy of the load is large enough exceeding the yield limit of amorphous diamond, the embedded amorphous diamonds fracture directly, intercepting the failure, as depicted in [Supplementary Figure 12](#). However, when the crack strength remains below a critical value required for initiating amorphous fracture, the energy is insufficient to destroy the diamond-like carbon particles, resulting in the blockage of crack tips at the boundaries. [Supplementary Figure 13](#) presents a model illustrating the fracture behavior of the crystalline-amorphous phase under indentation. This crystalline-amorphous system improves fracture resistance and contributes to excellent mechanical properties.

CONCLUSIONS

We investigated the structural evolution of the multi-walled BNNTs and C₆₀ mixture after recovery under HPHT conditions; a new type of crystalline-amorphous compound is synthesized with excellent mechanical properties. Characterizations demonstrated that the non-dense-phase boron nitride will reduce the mechanical properties of bulk materials. The crystalline-amorphous compound exhibited the excellent mechanical performance, with a Vickers' hardness of 86.2 GPa and fracture toughness of 10.2 MPa m^{1/2}. However, the polycrystalline c-BN and diamond compound caused the brittle failure compared to the crystalline-amorphous composite. The diamond-like carbon was uniformly embedded within the boron nitride dense phase. Furthermore, as crack tips migrated towards the boundaries between the amorphous and crystalline regions, they encountered obstruction and experienced significant bending. The diamond-like carbon particles in boron nitride dense phases can effectively hinder the continued cracking, thus enabling the crystalline-amorphous compound to have excellent mechanical properties.

DECLARATIONS

Authors' contributions

Experimental design: Gou H, Li J, Fang L

Synthesis of the sample: Li J, Niu G, Mu P, Yan B, Zhao S

Material testing: Niu G, Mu P, Liu F

Data analysis: Li J, Niu G, Mu P, Liu F

Original manuscript writing: Li J

Validation and original manuscript writing: Gou H, Fang L

Availability of data and materials

Not applicable.

Financial support and sponsorship

This work was supported by the National Science Fund for Distinguished Young Scholars (Grant No. T2225027) and the National Natural Science Foundation of China (Grant No. 12075215).

Conflicts of interest

All authors declared that there are no conflicts of interest.

Ethical approval and consent to participate

Not applicable.

Consent for publication

Not applicable.

Copyright

© The Author(s) 2024.

REFERENCES

1. Li G, Rahim MZ, Pan W, Wen C, Ding S. The manufacturing and the application of polycrystalline diamond tools - a comprehensive review. *J Manuf Process* 2020;56:400-16. [DOI](#)
2. Sahin Y, Motorcu AR. Surface roughness model in machining hardened steel with cubic boron nitride cutting tool. *Int J Refract Hard Mater* 2008;26:84-90. [DOI](#)
3. Wada T, Hanyu H. Tool wear of (Ti, Al) N-coated polycrystalline cubic boron nitride compact in cutting of hardened steel. *IOP Conf Ser Mater Sci Eng* 2017;264:012017. [DOI](#)
4. Sugihara T, Nishimoto Y, Enomoto T. Development of a novel cubic boron nitride cutting tool with a textured flank face for high-speed machining of inconel 718. *Precis Eng* 2017;48:75-82. [DOI](#)
5. Twardowski P, Legutko S, Krolczyk GM, Hloch S. Investigation of wear and tool life of coated carbide and cubic boron nitride cutting tools in high speed milling. *Adv Mech Eng* 2015;7:1687814015590216. [DOI](#)
6. Sahin Y. Comparison of tool life between ceramic and cubic boron nitride (CBN) cutting tools when machining hardened steels. *J Mater Process Technol* 2009;209:3478-89. [DOI](#)
7. Yallese MA, Chaoui K, Zeghib N, Boulanour L, Rigal J. Hard machining of hardened bearing steel using cubic boron nitride tool. *J Mater Process Technol* 2009;209:1092-104. [DOI](#)
8. Gastel M, Konetschny C, Reuter U, et al. Investigation of the wear mechanism of cubic boron nitride tools used for the machining of compacted graphite iron and grey cast iron. *Int J R Refract Hard Mater* 2000;18:287-96. [DOI](#)
9. Nagakubo A, Ogi H, Sumiya H, Hirao M. Elasticity and hardness of nano-polycrystalline boron nitrides: the apparent Hall-Petch effect. *Appl Phys Lett* 2014;105:081906. [DOI](#)
10. Zhao Z, Xu B, Tian Y. Recent advances in superhard materials. *Annu Rev Mater Res* 2016;46:383-406. [DOI](#)
11. Harris TK, Brookes EJ, Taylor CJ. The effect of temperature on the hardness of polycrystalline cubic boron nitride cutting tool materials. *Int J R Refract Hard Mater* 2004;22:105-10. [DOI](#)
12. Zunger A, Freeman AJ. *Ab initio* self-consistent study of the electronic structure and properties of cubic boron nitride. *Phys Rev B* 1978;17:2030-42. [DOI](#)
13. Solozhenko VL, Kurakevych OO, Le Godec Y. Creation of nanostructures by extreme conditions: high-pressure synthesis of ultrahard nanocrystalline cubic boron nitride. *Adv Mater* 2012;24:1540-4. [DOI](#) [PubMed](#)
14. Zhao M, Kou Z, Zhang Y, et al. Superhard transparent polycrystalline cubic boron nitride. *Appl Phys Lett* 2021;118:151901. [DOI](#)
15. Lu L, Shen Y, Chen X, Qian L, Lu K. Ultrahigh strength and high electrical conductivity in copper. *Science* 2004;304:422-6. [DOI](#)
16. Wen B, Xu B, Wang Y, et al. Continuous strengthening in nanotwinned diamond. *NPJ Comput Mater* 2019;5:117. [DOI](#)
17. Tian Y, Xu B, Yu D, et al. Ultrahard nanotwinned cubic boron nitride. *Nature* 2013;493:385-8. [DOI](#)
18. Shenderova OA, Brenner DW, Omeltchenko A, Su X, Yang LH. Atomistic modeling of the fracture of polycrystalline diamond. *Phys Rev B* 2000;61:3877-88. [DOI](#)
19. Sumiya H, Sakano F, Tatsumi N. Distribution of internal strain and fracture strength in various single-crystal diamonds. *Diam Relat Mater* 2023;134:109781. [DOI](#)
20. Schuh CA, Hufnagel TC, Ramamurty U. Mechanical behavior of amorphous alloys. *Acta Mater* 2007;55:4067-109. [DOI](#)
21. Liu Y, Zhou Y, Jia D, Yang Z, Li D, Liu B. Unveiling structural features and mechanical properties of amorphous Si₂BC₃N by density functional theory. *J Mater Sci Technol* 2023;139:103-12. [DOI](#)
22. Wang XJ, Lu YZ, Lu X, et al. Elastic criterion for shear-banding instability in amorphous solids. *Phys Rev E* 2022;105:045003. [DOI](#)
23. Dasgupta R, Hentschel HG, Procaccia I. Microscopic mechanism of shear bands in amorphous solids. *Phys Rev Lett* 2012;109:255502. [DOI](#) [PubMed](#)
24. Turnbull D, Cohen MH. Free-volume model of the amorphous phase: glass transition. *J Chem Phys* 1961;34:120-5. [DOI](#)
25. Abrosimova G, Chirkova V, Pershina E, Volkov N, Sholin I, Aronin A. The effect of free volume on the crystallization of Al₈₇Ni₈Gd₅ amorphous alloy. *Metals* 2022;12:332. [DOI](#)
26. Zhang S, Li Z, Luo K, et al. Discovery of carbon-based strongest and hardest amorphous material. *Natl Sci Rev* 2022;9:nwab140. [DOI](#) [PubMed](#) [PMC](#)
27. Li B, Ying P, Gao Y, et al. Heterogeneous diamond-CBN composites with superb toughness and hardness. *Nano Lett* 2022;22:4979-84. [DOI](#)
28. Liu Y, He D, Kou Z, et al. Hardness and thermal stability enhancement of polycrystalline diamond compact through additive

- hexagonal boron nitride. *Scr Mater* 2018;149:1-5. DOI
29. Pacella M, Axinte DA, Butler-smith PW, Shipway P, Daine M, Wort C. An assessment of the wear characteristics of microcutting arrays produced from polycrystalline diamond and cubic boron nitride composites. *J Manuf Sci Eng* 2016;138:021001. DOI
 30. Yin X, Kou Z, Wang Z, et al. Micro-sized polycrystalline cubic boron nitride with properties comparable to nanocrystalline counterparts. *Ceram Int* 2020;46:8806-10. DOI
 31. Xiang X, Guo Z, Chen Y, et al. Discovery of metastable W_3P single crystals with high hardness and superconductivity. *Inorg Chem* 2023;62:19279-87. DOI
 32. Huang Q, Yu D, Xu B, et al. Nanotwinned diamond with unprecedented hardness and stability. *Nature* 2014;510:250-3. DOI
 33. Solozhenko VL, Dub SN, Novikov NV. Mechanical properties of cubic BC_2N , a new superhard phase. *Diam Relat Mater* 2001;10:2228-31. DOI
 34. Meng Y, Mao HK, Eng PJ, et al. The formation of sp^3 bonding in compressed BN. *Nat Mater* 2004;3:111-4. DOI
 35. Bundy FP, Wentorf RH Jr. Direct transformation of hexagonal boron nitride to denser forms. *J Chem Phys* 1963;38:1144-9. DOI
 36. Hu M, He J, Zhao Z, et al. Compressed glassy carbon: an ultrastrong and elastic interpenetrating graphene network. *Sci Adv* 2017;3:e1603213. DOI PubMed PMC
 37. Shang Y, Liu Z, Dong J, et al. Ultrahard bulk amorphous carbon from collapsed fullerene. *Nature* 2021;599:599-604. DOI
 38. Tang H, Yuan X, Cheng Y, et al. Synthesis of paracrystalline diamond. *Nature* 2021;599:605-10. DOI
 39. Liu Y, Zhan GD, Wang Q, et al. Hardness of polycrystalline wurtzite boron nitride (wBN) compacts. *Sci Rep* 2019;9:10215. DOI PubMed PMC
 40. Matsumoto M, Huang H, Harada H, Kakimoto K, Yan J. On the phase transformation of single-crystal 4H-SiC during nanoindentation. *J Phys D Appl Phys* 2017;50:265303. DOI
 41. Guicciardi S, Melandri C, Monteverde FT. Characterization of pop-in phenomena and indentation modulus in a polycrystalline ZrB_2 ceramic. *J Eur Ceram Soc* 2010;30:1027-34. DOI
 42. Cai X, Xu Y, Zhong L, Liu M. Fracture toughness of WC-Fe cermet in W-WC-Fe composite by nanoindentation. *J Alloys Compd* 2017;728:788-96. DOI
 43. Gibson RF. A review of recent research on nanoindentation of polymer composites and their constituents. *Compos Sci Technol* 2014;105:51-65. DOI
 44. Langenhorst F, Solozhenko VL. ATEM-EELS study of new diamond-like phases in the B-C-N system. *Phys Chem Chem Phys* 2002;4:5183-8. DOI
 45. Egerton RF, Malac M. EELS in the TEM. *J Electron Spectrosc Relat Phenomena* 2005;143:43-50. DOI
 46. Reddy SM, Timms NE, Trimby P, Kinny PD, Buchan C, Blake K. Crystal-plastic deformation of zircon: a defect in the assumption of chemical robustness. *Geology* 2006;34:257-60. DOI